

Tsunamigenic structures in a creeping section of the Alaska subduction zone

Anne Bécel^{1*}, Donna J. Shillington¹, Matthias Delescluse², Mladen R. Nedimović^{1,3}, Geoffrey A. Abers⁴, Demian M. Saffer⁵, Spahr C. Webb¹, Katie M. Keranen⁴, Pierre-Henri Roche², Jiyao Li¹ and Harold Kuehn³

Segments of subduction zones that are capable of generating tsunamigenic earthquakes appear to have characteristic structural configurations. These structures include heterogeneous plate interfaces, a small wedge of deformed sediment at the toe of the overriding plate (the frontal prism), and splay faults in the crust of the overriding plate that root within the plate boundary megathrust. Here we use seismic reflection imaging to show that these features also exist within a creeping segment of the Alaska subduction zone, the Shumagin Gap. We identify an active crustal-scale normal fault system that dips landward and resembles that involved in the 2011 Tohoku-oki earthquake in Japan. We also find that the Shumagin Gap has a small frontal prism, a deep-water splay fault, and that the plate interface here is rough and thinly sedimented. We propose that lateral propagation of rupture from a neighbouring segment into the Shumagin Gap may explain a tsunamigenic earthquake that occurred there in 1788 and that tsunamigenic potential should be considered in hazard assessments for the region. Our results demonstrate that structural configurations similar to those in Tohoku may exist in other subduction zones, including within creeping segments or segments with no record of historical megathrust earthquakes, but are under-recognized. Identifying similar configurations globally may improve our ability to anticipate regions capable of generating large tsunamis.

Slip on the shallow portion of subduction zone plate boundary faults can trigger very large tsunamis. This can occur when large interplate earthquakes propagate to the trench or during ‘tsunami earthquakes’, a special class of earthquakes that produce larger tsunamis than expected for their moment magnitude¹ and are characterized by low rupture velocities and long durations. Both types of event primarily occur at subduction zones that have a small frontal prism, a thin layer of subducting sediment and highly faulted oceanic crust^{2–4}. The most dramatic recent example of shallow, tsunamigenic slip occurred during the 2011 Tohoku-oki earthquake³; over 50 m of slip occurred near the trench, resulting in local tsunami run-up up to 30 m. This earthquake highlighted another important feature that can be associated with tsunamigenic slip—a landward-dipping, localized normal fault branching from the megathrust. Extension is expected in the overriding plate when earthquake rupture propagates to shallow depths^{5,6}. Alternatively, studies of the Tohoku-oki earthquake suggest that this normal fault may actively promote shallow slip by decoupling the portion of the wedge located seaward of the normal fault^{7,8}. Shallow slip in great earthquakes and/or tsunami earthquakes is rare but very destructive, making it imperative to extract any information on structures that are associated with these events, such as the Tohoku normal fault, and apply it to the global subduction zone system. To date, only a few normal faults branching from the megathrust have been identified^{3,9,10}. This may be because these faults are steep, extend to great depths, and in many subduction zones straddle the shoreline making them challenging to image and because their significance was not appreciated until the Tohoku event.

There is also growing evidence that even creeping or weakly seismically coupled subduction zone segments may host tsunamigenic earthquakes (for example, Java¹¹; Nicaragua^{12,13}). Examples of such events along the Alaska–Aleutian margin are the $M_{8.6}$ 1957 earthquake that propagated laterally through a weakly coupled shallow portion of the megathrust offshore Unalaska Island, causing an unusually large (23 m) tsunami¹⁴, and the $M_w 8.6$ tsunami earthquake in 1946¹⁵ that ruptured the weakly coupled segment offshore Unimak Island (Fig. 1). These and other events in weakly coupled segments highlight the importance of considering potentially tsunamigenic structural configurations in segments thought to be creeping or with no record of historical megathrust earthquakes.

Current knowledge of the Shumagin Gap

We focus on the ~200-km-wide Shumagin Gap, which has not ruptured in a great earthquake in 150 years¹⁶ (Fig. 1). GPS (Global Positioning System) data indicate that this segment is creeping to weakly locked, although coupling on the shallow part of the plate boundary is not well resolved by the onshore data¹⁷. Over the last century, a few moderate earthquakes ($M_{6.5}$ to $M_{7.5}$) have occurred in the area at depths greater than 35 km (Fig. 1). Some authors suggest that instead of rupturing in one large earthquake, most of the seismic moment in the Shumagin Gap is released through steady creep and thus a moderate $M \sim 7$ earthquake every ~40 years, as observed in the last century, is sufficient to accommodate the residual slip deficit¹⁷. However, earthquakes in 1788 and possibly 1847 are inferred to have ruptured laterally through part or all of the Shumagin Gap¹⁶. The 1788 earthquake ruptured from the

¹Lamont-Doherty Earth Observatory of Columbia University, Palisades, New York 10964, USA. ²Ecole Normale Supérieure, UMR 8538, PSL Research University, 75231 Paris, France. ³Dalhousie University, Halifax, Nova Scotia B3H 4R2, Canada. ⁴Cornell University, Ithaca, New York 14853, USA. ⁵Penn State, University Park, Pennsylvania 16802, USA. *e-mail: annebcl@ldeo.columbia.edu

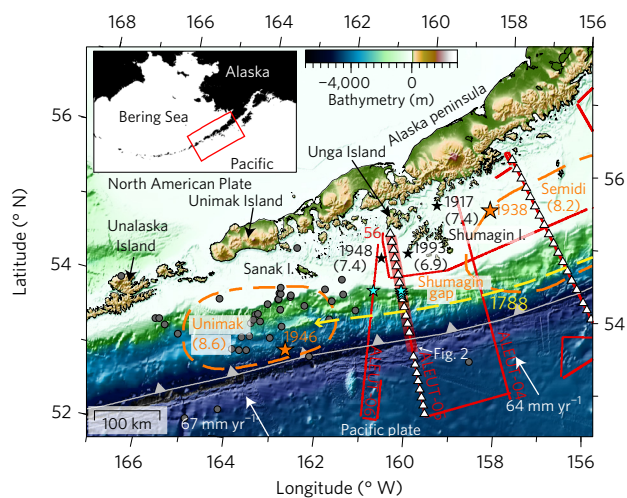


Figure 1 | Tectonic setting and extent of the Sanak and Unimak basins.

Map of the subduction zone off the Alaska Peninsula. MCS profiles from the ALEUT experiment are shown with red lines; ocean bottom seismometers (OBSs) are represented by white triangles. Dashed orange lines and stars denote the rupture area of the 1946¹⁵ and 1938 earthquakes¹⁶ and their epicentres. The yellow dashed line indicates the rupture extent of the 1788 earthquake^{16,22}. Aftershocks from the 1946 earthquakes are shown by dark grey circles. Moderate earthquakes ($M_{6.9-7.5}$) that occurred in the last century are represented by black stars. Cyan stars show fault locations at the seafloor from new seismic and bathymetry data acquired from this study. The light grey line marks the trench³⁸. Convergence vectors are in white³⁹. The inset shows the general location of the study area relative to North America.

neighbouring Semidi segment¹⁶, which is currently strongly coupled. Historical records suggest that the 1788 earthquake, in particular, generated a large tsunami¹⁶. The importance of recognizing the hazard posed by the weakly coupled Shumagin Gap was emphasized by a recent tsunami scenario for the Alaska subduction zone¹⁸ showing that a large tsunami in this segment could have devastating consequences to coastal communities locally in Alaska and around the Pacific Ocean.

Structural configuration of the Shumagin Gap

We present new observations of the Shumagin Gap in the Alaska Peninsula from multichannel seismic (MCS) reflection, wide-angle reflection/refraction, and bathymetric data acquired using the RV *Marcus G. Langseth* in the summer of 2011 during the ALEUT (Alaska Langseth Experiment to Understand the megaThrust) programme. MCS data were acquired using two 8-km-long seismic streamers and a 6600 cu. in. tuned airgun array.

The MCS data clearly reveal a structural configuration in the Shumagin Gap that could make it prone to generating both transoceanic and local tsunamis and that can explain past events generated by this presumed creeping segment. We observe a large, active normal fault that may either slip coseismically allowing displacement over a large area seaward of the fault⁷ or be triggered by shallow earthquake rupture propagation⁶, as determined for the Tohoku earthquake^{3,9}, and thus could either promote or result from shallow slip. We also observe a heterogeneous character along the shallow plate boundary, a small frontal prism and a deep-water thrust splay fault, all of which are favourable to tsunamigenesis¹⁹.

As mentioned above, the most prominent feature imaged is a large, landward-dipping normal fault in the overriding plate that bounds the eastern Sanak Basin. This fault system crosses the upper slope 75 km from the trench, dips $\sim 40^\circ-45^\circ$, cuts the entire crust and connects to the plate boundary fault at ~ 35 km depth, near the intersection of the megathrust with the forearc mantle wedge (Fig. 2

and Supplementary Figs 1–5). The fault splays into two branches around ~ 6 km depth, which breach the seafloor at water depths of $\sim 500-700$ m. The association of this fault system with the ~ 6 -km-thick, Miocene Sanak Basin²⁰ (Fig. 1b) suggests that the fault has had sustained activity and accommodated significant total normal displacement (Fig. 2b). The offset of the acoustic basement is very significant (~ 2 km), which is an indication of the cumulative slip on the fault. Farther northeast in the strongly coupled Semidi segment (Fig. 1) that ruptured in a $M_{8.2}$ earthquake in 1938, the sediment on the upper slope is much thinner, and no major deep basin or branching normal fault system is imaged in the overriding plate²¹. The epicentre of the 1938 Semidi earthquake was deep, and this earthquake did not appear to reach the trench and thus produced only a small tsunami²².

The new data presented here also demonstrate that the fault bounding the Sanak Basin and connecting to the plate boundary fault has recently been active (Fig. 2). The fault offsets the youngest sediments, and ~ 5 -m-high scarps are observed at the seafloor in multibeam bathymetry data (Fig. 2c). Observed pockmark features near the surface expression of the fault and perturbed sediments could suggest localized fluid flow (Fig. 2b,c and Supplementary Fig. 6). A cluster of earthquakes occurs at the intersection of this fault with the main plate boundary fault, and some seismicity also occurs within the upper plate near the fault and farther landward (Fig. 2a)²³.

The properties of the shallow plate boundary and structures in the overriding plate near the trench in the Shumagin Gap are also constrained by the seismic reflection data. These features are consistent with settings known to generate tsunami earthquakes. The incoming oceanic plate has a thin (50–800 m) and irregular sediment cover that is strongly disrupted by bending faulting²⁴. Only $\sim 250-500$ m of sediment appear to be subducting, and can only be traced ~ 10 km from the trench. Farther landward, the megathrust itself is marked by a discontinuous reflection, and we image clear older thrust faults in the outer wedge that merge with the top of oceanic crust (Fig. 3). The most landward thrust fault is located 20 km from the trench and merges with the megathrust at ~ 12 km depth (Fig. 3b). This prominent fault separates a highly deformed outer wedge with clearly imaged thrust faults from ‘transparent’ basement rocks farther landward that are overridden by tilted slope sediment (Fig. 3b).

Implications of imaged structures for tsunamigenesis

The newly documented structures in the overriding plate and plate boundary properties, taken together, could provide a recipe for tsunamigenesis accompanying earthquakes in the weakly coupled Shumagin Gap. Margins characterized by thin subducting sediment, a small frontal prism and heterogeneous plate interface at shallow depth and are widely believed to be prone to both slow earthquakes and tsunamigenesis^{19,25}. The deep-water splay fault near the trench and/or the rough, shallow plate interface would favour the generation of a transoceanic tsunami²⁶. The rough surface of the plate interface itself near the trench with sediment trapped in fault-generated topography at the top of the oceanic crust could favour erratic and slow rupture propagation, as proposed for the 1896 Sanriku tsunami earthquake²⁷ or the occurrence of slow slip events²⁸. The narrow frontal prism also implies that lithified materials (including basement rocks) are present near the trench, and therefore could permit the storage of elastic strain that could lead to coseismic slip on the shallow part of the subduction zone and that could favour large far-field tsunamis as proposed for other subduction zones^{2,29}.

Following the Tohoku earthquake, several studies have shown that a deeply rooted active normal fault within the overriding plate may be an indicator of rupture propagation to the trench^{3,5,6} because large slip on the shallow plate interface would drive extension in the overriding plate^{5,6}. If the normal fault system is activated by a

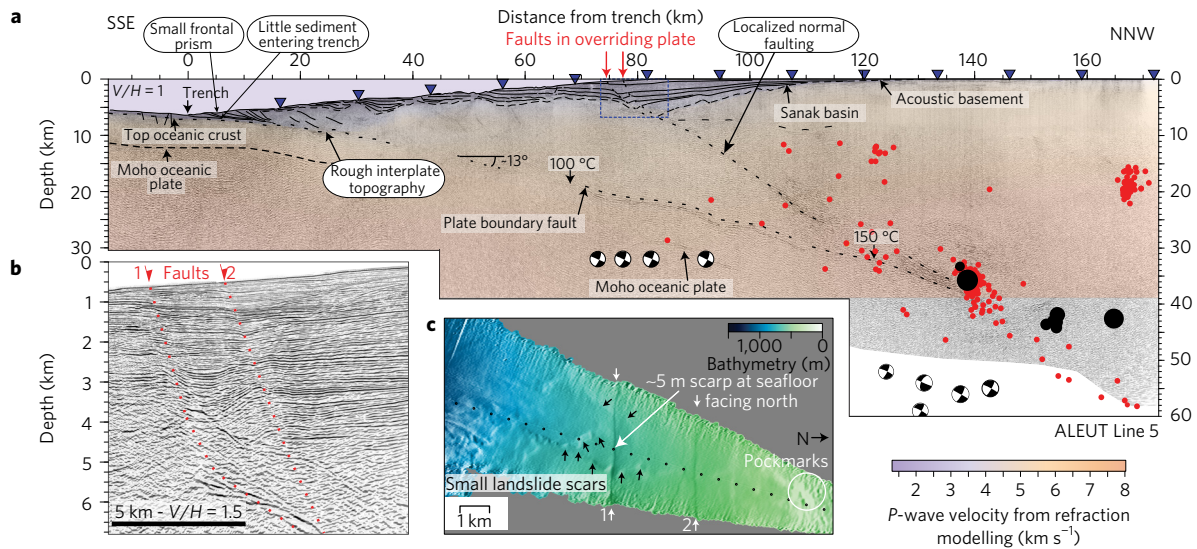


Figure 2 | Reflection image and bathymetry profile for ALEUT Line 5. **a**, Reflection image of ALEUT Line 5 superimposed on a first-arrival tomographic model from OBS data. OBS are represented by inverted blue triangles. Earthquakes that occurred within 15 km of the profile have been projected laterally onto the profile. Red and black dots are the small earthquakes and notable events with thrust mechanisms ($3.0 < M < 6.8$) (ref. 40) recorded by the Shumagin Network (see Supplementary Fig. 7 for locations)²³; events with focal mechanisms are from the Centroid Moment Tensor catalogue. Slab temperatures are taken from ref. 33. **b**, Magnification of the section of the pre-stack depth-migrated reflection image outlined in **a** with a blue dashed line showing the shallow part of the fault system and **c**, Bathymetry across this fault system with ~ 5 m scarp.

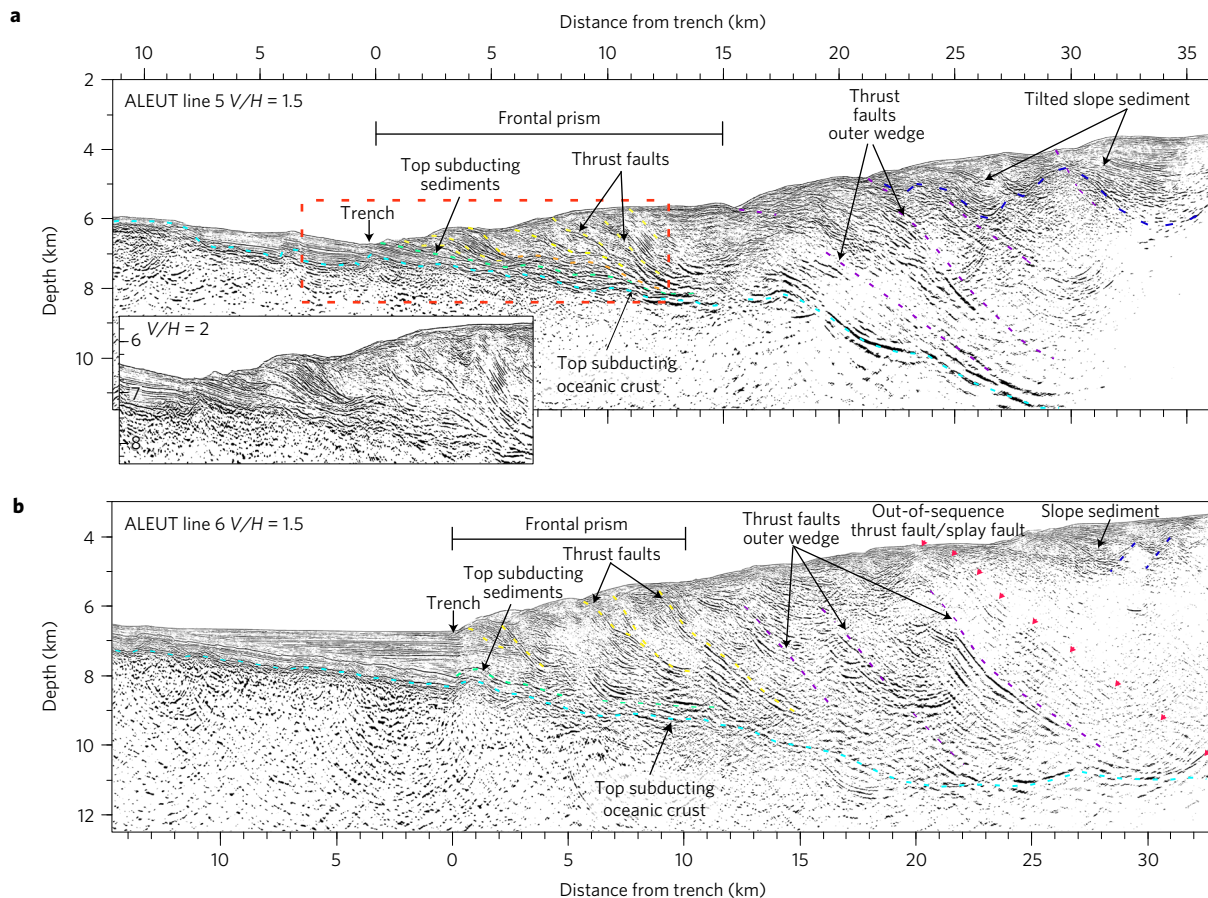


Figure 3 | Lower slope of ALEUT Lines 5 and 6. **a, b**, Pre-stack depth-migrated reflection images of the structure of the lower slope for ALEUT Line 5 (**a**) and ALEUT Line 6 (**b**). Inset: Magnification of the section of the pre-stack depth-migrated reflection image outlined with a red dashed line in **a**.

large earthquake, it could allow for the decoupling of the wedge seaward of the normal fault, thus allowing shallow slip and uplift of the seafloor⁷ leading to the release of gravitational potential energy

over a large area or enabling dynamic overshoot^{8,30}. The normal fault involved in the Tohoku earthquake appears to separate parts of the seafloor that experienced very different amounts of horizontal

motion (5–30 m of horizontal motion landward of the fault and 58–74 m of horizontal motion seaward of the normal fault) though the normal fault itself appears to have slipped only by 1 m during the earthquake³⁰. Normal faults in the overriding plate could be activated at steeply tapered outer wedges during large earthquakes by the reduction in basal traction associated with stress drops³¹.

The normal fault system in the Shumagin Gap appears to mark a clear boundary in the distribution of the seismicity, where abundant plate interface seismicity is observed landward of the intersection of this fault with the megathrust, but less seismic activity occurs seaward of the intersection (Fig. 2 and Supplementary Fig. 7). The change observed in seismicity is robust and not related to station distribution (see Supplementary Fig. 8 and Methods). The sharp change in seismicity where this fault intersects the megathrust implies that it could be associated with a change in the physical properties of the upper plate or conditions and frictional behaviour of the plate interface. Recent studies suggest that changes in frictional parameters are required to localize normal faulting along a major fault³¹. More specifically, those studies indicate a lower effective friction on the plate interface updip of the normal fault than downdip of this fault. A heterogeneous plate interface is known to facilitate activation of branching faults above the megathrust³².

Slip on the major, active landward-dipping normal fault system imaged in the Shumagin Gap, which is located 75 km from the trench, is also expected to produce vertical displacement of the seafloor near the fault in addition to decoupling the seaward portion of the wedge, and thus could enhance the local tsunami, although this effect is known to be smaller than the rupture propagating to the trench⁵ and strongly depends on bathymetric effects.

Comparing thermal models for the subduction zone off the Alaska Peninsula³³ with the structural configuration imaged here and the estimated ruptures of past earthquakes suggests that temperature is not the primary control on slip behaviour here. In our study area, the 150 °C isotherm, which is hypothesized to represent the updip limit of ruptures in some subduction zones³⁴, lies ~120 km from the trench at a depth of 30 km, deeper than estimated great earthquake ruptures in this region (for example, during the 1938 earthquake)^{21,22}. This is similar to other relatively cold subduction zones, such as Tohoku, where temperature also does not appear to be an important control.

The structural configuration observed for the Shumagin Gap would make this segment particularly prone to producing tsunamigenic slip, but what causes coseismic slip capable of producing tsunamis to occur in a creeping or weakly coupled section is not clear. Past earthquakes suggest that ruptures can propagate laterally into the Shumagin Gap from neighbouring locked segments. On 7 August 1788, a tsunamigenic earthquake occurred in the Shumagin segment¹⁶. Based on historical descriptions from Russian settlers, wave heights of tens of metres have been reported on Sanak and Unga Islands (Fig. 1), similar to the wave height recorded for the 1946 Unimak near-field tsunami. We suggest that the shallow plate boundary and/or splay faults in the overriding plate in this creeping to weakly coupled section may have moved coseismically when the 1788 earthquake propagated into the shallow Shumagin Gap. Other past events demonstrate that asperities can ultimately break through a neighbouring creeping to weakly coupled segment. During the last 15 years, significant seismological evidence of rupture propagation laterally through creeping segments³⁵ or updip, through part of the subduction interface that is thought to be weakly coupled³⁶, has accumulated. For example, the 1964 Alaska earthquake ruptured two large asperities but also a weakly coupled segment between those asperities³⁷, and the 1957 Alaska Earthquake ruptured the weakly coupled Unalaska segment¹⁴.

The possibility of lateral propagation of earthquakes nucleated in the neighbouring locked Semidi segment into the Shumagin Gap, where we show a structural architecture favourable to large local

and transoceanic tsunamis, needs to be taken into account when considering hazards for this region. Rupture propagation through the creeping to weakly coupled Shumagin Gap and activation of the normal fault system leading to either release of gravitational energy or amplified motion seaward of this fault by dynamic overshooting would result in greater tsunamigenic potential for this segment than the elastic coupling estimates predict^{7,31}. This, if not taken into account, could result in an under-estimation of the seismic hazard.

This study demonstrates that normal faults comparable to the one involved in the Tohoku earthquake are present in other subduction zones. Such faults may be under-recognized globally because their significance for tsunamigenesis was previously not appreciated given the rarity of shallow slip in the short historical record, and because seismically imaging these structures requires modern long-offset, large source MCS data, which are available only on a small number of subduction zones. Additionally, if such structures straddle the shoreline, they would not be detected by imaging efforts.

It also suggests that creeping regions might have greater tsunami potential than previously recognized. Identifying and characterizing active crustal-scale normal faults in the overriding plate as promoters or indicators of rupture to the trench, and the shallow megathrust configuration is thus essential to a complete and comprehensive understanding of hazards in the global subduction system.

Methods

Methods, including statements of data availability and any associated accession codes and references, are available in the [online version of this paper](#).

Received 22 December 2016; accepted 21 June 2017;
published online 24 July 2017

References

- Kanamori, H. Mechanism of tsunami earthquakes. *Phys. Earth Planet. Inter.* **6**, 346–359 (1972).
- Polet, J. & Kanamori, H. Shallow subduction zone earthquakes and their tsunamigenic potential. *Geophys. J. Int.* **142**, 684–702 (2000).
- Tsuji, T. *et al.* Extension of continental crust by anelastic deformation during the 2011 Tohoku-oki earthquake: the role of extensional faulting in the generation of a great tsunami. *Earth Planet. Sci. Lett.* **364**, 44–58 (2013).
- Okamura, Y. *et al.* Fore arc structure and plate boundary earthquake sources along the southwestern Kuril subduction zone. *J. Geophys. Res.* **113**, B06305 (2008).
- Li, S. Y., Moreno, M., Rosenau, M., Melnick, D. & Oncken, O. Splay fault triggering by great subduction earthquakes inferred from finite element models. *Geophys. Res. Lett.* **41**, 385–391 (2014).
- Xu, S. Q., Fukuyama, E., Yue, H. & Ampuero, J. P. Simple crack models explain deformation induced by subduction zone megathrust earthquakes. *Bull. Seismol. Soc. Am.* **106**, 2275–2289 (2016).
- McKenzie, D. & Jackson, J. Tsunami earthquake generation by the release of gravitational potential energy. *Earth Planet. Sci. Lett.* **345**, 1–8 (2012).
- Ide, S., Baltay, A. & Beroza, G. C. Shallow dynamic overshoot and energetic deep rupture in the 2011 M-w 9.0 Tohoku-Oki earthquake. *Science* **332**, 1426–1429 (2011).
- Tsuji, T. *et al.* Potential tsunamigenic faults of the 2011 off the Pacific coast of Tohoku Earthquake. *Earth Planets Space* **63**, 831–834 (2011).
- Klaeschen, D., Belykh, I., Gribidenko, H., Patrikeyev, S. & Vonhuene, R. Structure of the Kuril trench from seismic-reflection records. *J. Geophys. Res.* **99**, 24173–24188 (1994).
- Bilek, S. L. & Engdahl, E. R. Rupture characterization and aftershock relocations for the 1994 and 2006 tsunami earthquakes in the Java subduction zone. *Geophys. Res. Lett.* **34**, L20311 (2007).
- Satake, K. Mechanism of the 1992 Nicaragua tsunami earthquake. *Geophys. Res. Lett.* **21**, 2519–2522 (1994).
- Correa-Mora, F. *et al.* GPS-derived coupling estimates for the Central America subduction zone and volcanic arc faults: El Salvador, Honduras and Nicaragua. *Geophys. J. Int.* **179**, 1279–1291 (2009).
- Nicolisky, D., Freymueller, J., Witter, R., Suleimani, E. & Koehler, R. Evidence for shallow megathrust slip across the Unalaska seismic gap during the great 1957 Andreanof Islands earthquake, eastern Aleutian Islands, Alaska. *Geophys. Res. Lett.* **43**, 10328–10337 (2016).

15. Lopez, A. M. & Okal, E. A. A seismological reassessment of the source of the 1946 Aleutian 'tsunami' earthquake. *Geophys. J. Int.* **165**, 835–849 (2006).
16. Davies, J., Sykes, L., House, L. & Jacob, K. Shumagin seismic gap, Alaska Peninsula—history of great earthquakes, tectonic setting, and evidence for high seismic potential. *J. Geophys. Res.* **86**, 3821–3855 (1981).
17. Fournier, T. J. & Freymueller, J. T. Transition from locked to creeping subduction in the Shumagin region, Alaska. *Geophys. Res. Lett.* **34**, L06303 (2007).
18. Kirby, S., Scholl, D., von Huene, R. & Wells, R. *Alaska Earthquake Source for the SAFRR Tsunami Scenario: Chapter B in The SAFRR (Science Application for Risk Reduction) Tsunami Scenario* 33–79 (Report No. 2331–1258, US Geological Survey, 2013).
19. Wang, K. L. & Bilek, S. L. Invited review paper: fault creep caused by subduction of rough seafloor relief. *Tectonophysics* **610**, 1–24 (2014).
20. Bruns, T. R., von Huene, R., Culotta, R. C., Lewis, S. D. & Ladd, J. W. in *Geology and Resource Potential of the Continental Margin of Western North America and Adjacent Ocean Basins, Beaufort Sea to Baja California* Vol. 6 (eds Scholl, D. W., Grantz, A. & Vedder, J.) Ch. 8, 157–190 (Circum-Pacific Council for Energy and Mineral Resources, 1987).
21. Li, J. Y. *et al.* Downdip variations in seismic reflection character: implications for fault structure and seismogenic behavior in the Alaska subduction zone. *J. Geophys. Res.* **120**, 7883–7904 (2015).
22. Estabrook, C. H., Jacob, K. H. & Sykes, L. R. Body wave and surface-wave analysis of large and great earthquakes along the eastern Aleutian Arc, 1923–1993—implications for future events. *J. Geophys. Res.* **99**, 11643–11662 (1994).
23. Abers, G. A. Relationship between shallow-depth and intermediate-depth seismicity in the eastern Aleutian subduction zone. *Geophys. Res. Lett.* **19**, 2019–2022 (1992).
24. Shillington, D. J. *et al.* Link between plate fabric, hydration and subduction zone seismicity in Alaska. *Nat. Geosci.* **8**, 961–964 (2015).
25. Bilek, S. L. The role of subduction erosion on seismicity. *Geology* **38**, 479–480 (2010).
26. Moore, G. F. *et al.* Three-dimensional splay fault geometry and implications for tsunami generation. *Science* **318**, 1128–1131 (2007).
27. Tanioka, Y., Ruff, L. & Satake, K. What controls the lateral variation of large earthquake occurrence along the Japan Trench? *Island Arc* **6**, 261–266 (1997).
28. Saffer, D. M. & Wallace, L. M. The frictional, hydrologic, metamorphic and thermal habitat of shallow slow earthquakes. *Nat. Geosci.* **8**, 594–600 (2015).
29. Contreras-Reyes, E., Flueh, E. R. & Grevemeyer, I. Tectonic control on sediment accretion and subduction off south central Chile: implications for coseismic rupture processes of the 1960 and 2010 megathrust earthquakes. *Tectonics* **29**, TC6018 (2010).
30. Ito, Y. *et al.* Frontal wedge deformation near the source region of the 2011 Tohoku-Oki earthquake. *Geophys. Res. Lett.* **38**, L00G05 (2011).
31. Cubas, N., Avouac, J. P., Leroy, Y. M. & Pons, A. Low friction along the high slip patch of the 2011 M_w 9.0 Tohoku-Oki earthquake required from the wedge structure and extensional splay faults. *Geophys. Res. Lett.* **40**, 4231–4237 (2013).
32. Wendt, J., Oglesby, D. D. & Geist, E. L. Tsunamis and splay fault dynamics. *Geophys. Res. Lett.* **36**, L15303 (2009).
33. Syracuse, E. M., van Keken, P. E. & Abers, G. A. The global range of subduction zone thermal models. *Phys. Earth Planet. Inter.* **183**, 73–90 (2010).
34. Hyndman, R. D. & Wang, K. Thermal constraints on the zone of major thrust earthquake failure—the cascadia subduction zone. *J. Geophys. Res.* **98**, 2039–2060 (1993).
35. Ammon, C. J. *et al.* Rupture process of the 2004 Sumatra-Andaman earthquake. *Science* **308**, 1133–1139 (2005).
36. Noda, H. & Lapusta, N. Stable creeping fault segments can become destructive as a result of dynamic weakening. *Nature* **493**, 518–521 (2013).
37. Freymueller, J. T. *et al.* *Active Tectonics and Seismic Potential of Alaska* 1–42 (American Geophysical Union, 2008).
38. Bird, P. An updated digital model of plate boundaries. *Geochem. Geophys. Geosyst.* **4**, 1027 (2003).
39. Sella, G. F., Dixon, T. H. & Mao, A. L. REVEL: a model for recent plate velocities from space geodesy. *J. Geophys. Res.* **107**, ETG 11-1–ETG-11-30 (2002).
40. Abers, G. A., Hu, X. X. & Sykes, L. R. Source scaling of earthquakes in the Shumagin region, Alaska—time-domain inversions of regional wave-forms. *Geophys. J. Int.* **123**, 41–58 (1995).

Acknowledgements

We gratefully acknowledge the captain, technical staff and crew of the RV *Marcus G. Langseth* and the Scripps OBS team who made this data set possible. This work was supported by the US National Science Foundation grants OCE-0926614 and EAR-1347312.

Author contributions

D.J.S., M.R.N. and S.C.W. obtained funding for the marine seismic programme. D.J.S., A.B., M.R.N., S.C.W. and M.D. collected marine data during the research cruise on RV *Langseth*. A.B., G.A.A., K.M.K., D.J.S., M.R.N. and D.M.S. obtained funding for seismicity and seismic data integration. A.B. conducted the MCS processing. D.J.S. performed the wide-angle reflection/refraction modelling. K.M.K. and G.A.A. analysed the seismicity data. All authors discussed the results and commented on the manuscript.

Additional information

Supplementary information is available in the [online version of the paper](#). Reprints and permissions information is available online at www.nature.com/reprints. Publisher's note: Springer Nature remains neutral with regard to jurisdictional claims in published maps and institutional affiliations. Correspondence and requests for materials should be addressed to A.B.

Competing financial interests

The authors declare no competing financial interests.

Methods

MCS data analysis. Processing of MCS data was conducted with Echos and Geodepth software packages from Paradigm Geophysical. Data were processed using the following sequence: a three-dimensional (3D) pseudo geometry was assigned to preserve the true receiver–source offsets with binning of the data into 6.25-m bins, noise was removed using the LIFT method⁴¹, a bandpass filtering (3–7–100–125 Hz), a spherical divergence correction and a predictive deconvolution to remove reverberations were then applied. For multiple attenuation, we used a combination of surface-related multiple elimination technique in the shot point domain and linear and parabolic radon transforms in common mid-point (CMP) supergather domain to remove residual multiples. Semblance-type velocity analysis was conducted at every 480th CMP (3 km). After applying normal moveout corrections and stacking, a Kirchhoff post-stack time migration was applied to the data using a smoothed version of the r.m.s. velocities. A bandpass filter with time- and space-varying frequencies was then applied based on the imaged geologic structures, as well as a time- and space-varying gain for display. A Kirchhoff pre-stack depth migration algorithm (Eikonal) was later applied to selected portions of the profiles. The starting velocity model for pre-stack depth migration was based on the picked r.m.s. velocities. This model was converted to depth and updated iteratively using residual velocity analysis in the depth domain at every 100th common reflection point (~0.625 km).

Bathymetry data analysis. Multibeam bathymetry data processing was performed using MB-system⁴². The processing steps include ping editing, spike removal with a beam-to-beam maximum angle of 50°, and limits on depth and swath width using local mean. The bathymetry data were used to characterize the orientation and relief of a fault system associated with the deep Sanak Basin located on ALEUT Lines 5 and 6.

Wide-angle reflection/refraction data analysis. Ocean bottom data processing consisted of a 3–5–15–20 Hz minimum-phase bandpass filter, range-varying gains and predictive deconvolution. Data from OBS located on the overriding plate on ALEUT Line 5 exhibit clear crustal turning compressional waves (Pg) in the overriding plate at offsets up to ~90 km (for example, OBS 517, 521, Supplementary Fig. 3), reflections from the base of the overriding plate, top of the subducting slab, and the Moho of the subducting slab at variable offsets and mantle refraction (Pn) in the upper mantle of the subducting plate up to offsets up to ~180 km. Most importantly for this study, reversed wide-angle reflections from the Moho of the overriding plate where it overlies the forearc mantle wedge are observed on four OBS receiver gathers (Supplementary Fig. 3c–f). We assigned uncertainties of 30–125 ms to the travel time picks, with larger uncertainties assigned to deep reflections and long-offset refractions.

The objectives of velocity modelling presented here were twofold: to obtain a relatively smooth, but reliable, velocity model for depth-converting seismic reflection data; and to explore the relationship between the large normal fault, megathrust and base of the overriding plate. For the former, we used a regularized tomographic inversion of travel time picks using Jive3D⁴³ to create a P-wave velocity model (Supplementary Fig. 2). In this model, layers were included for the water column and sediments and held fixed during the inversion. Sediment velocities were taken from smoothed r.m.s. velocities converted to interval velocities. Grid spacing is 1 km × 0.5 km in the crust. Smoothing constraints are set to apply a factor of 2 more horizontal than vertical smoothing. The final first arrival velocity model has an r.m.s. travel time residual of 96 ms and a chi-squared misfit of 1.77. We allowed a larger misfit to obtain a smooth, simple model for depth conversion.

In a second step, to further explore the relationship of the normal fault, the megathrust and the Moho of the overriding plate, we have performed forward modelling of deep wide-angle reflection arrivals using RAYINVR⁴⁴. We developed a relatively simple, layered velocity model of the landward part of the subduction zone based on the results of the tomographic inversion described above. This model is based on refractions through the sediments and crust, reflections off the top of basement, an intracrustal reflector and reflections off the base of the crust and megathrust. The crust has two layers with velocities between 6.0 and 6.8 km s⁻¹. This model shows that the megathrust diverges from the Moho of the overriding plate at 30–35 km (increasing in depth landward). This is consistent with receiver function results farther north onshore⁴⁵, which give a crustal thickness of 39 km. This model uses 1,168 picks and has an overall misfit of 127 ms. The Pg arrivals have a misfit of 111 ms, χ^2 of 1.9, and the Moho and megathrust reflections have a misfit of 197 ms. This very simple model demonstrates that the megathrust diverges from the base of the crust of the overriding plate approximately where the normal fault in the overriding plate meets the megathrust.

Seismicity analysis. The Shumagin network comprised 19 seismometers from the outer Shumagin Islands to the Bering Sea (See Supplementary Fig. 7 for locations). This network operated digitally from 1982 to 1991. Stations were linked by analogue telemetry to the seismic station called SAN (see Supplementary Fig. 7 for location) and recorded by triggering on a 12-bit digital system. Previously,

earthquakes were relocated in a joint inversion for 3D velocity structure^{23,46} (Supplementary Fig. 7A). In this study, earthquakes that were not in the original catalogue²³ were relocating in the 3D model from ref. 46 using a single-event location procedure. This reanalysis uses events with fewer recordings per event, and about doubles the number of high-quality locations from just over 1,440 to about 2,800 (Supplementary Fig. 7b). The vertical uncertainty of the earthquake on Line 5 is ~3–5 km at depths >20 km.

The major normal fault system imaged in the overriding plate appears to exert a strong control on the seismicity, both on the megathrust and in the overriding plate. Seaward of the fault system, the seismicity has a low occurrence rate, whereas landward of this fault, seismicity is frequent both on the downdip portion of the megathrust and the overlying plate. To verify that this change is not related to the station distribution in this area, we estimate the minimum magnitude of catalogue completeness (MC) across the Shumagin segment by searching for departures from the linear frequency–magnitude relationship⁴⁷ using 100 × 100 km bins as in ref. 24. We use the Alaska Earthquake Information Center (AEIC) catalogue for the estimation that shows the same clear change in the distribution of earthquakes across the fault (Supplementary Fig. 8, panel a). The AEIC catalogue is based on a network of stations deployed throughout Alaska for the past 10–20 years. The station distribution is uneven, and we thus expect the detection threshold to be heterogeneous. Results show that in the Shumagin Gap, along ALEUT MCS Line 5, MC varies from ~2.5–3 near the trench to ~1.5–2 at 50 km landward from the trench for earthquakes with depths less than 50 km (Supplementary Fig. 8b). The observation that there is very little seismicity with magnitude greater than ~2.5 down to 25 km depth is thus not related to the station distribution in this area.

Uncertainty on the depth of the plate interface. To assess the depth uncertainties in the reflection image of the major landward-dipping normal fault and the plate boundary fault, we compare the depth of both faults on the time-migrated ALEUT Line 5 converted to depth using a suite of velocity models available in the Shumagin segment (Supplementary Fig. 9). The different velocity models used are: (1) the first arrival tomographic model with the velocities within the sediment being interval velocities derived from a smooth version of the r.m.s. velocities picked on the reflection data. These smooth interval velocities were converted to depth and kept fixed during the inversion; (2) the tomographic model that takes into account secondary deep arrivals; (3) the 2.5D velocity model from the earthquake tomography⁴⁶; (4) the 1D gradient velocity model⁴⁶ for which the seafloor and sediment velocities were added as described for (1); and (5) the 1D step velocity model⁴⁶ for which the seafloor and sediment velocities were added as described for (1). Results show that the plate boundary fault has depth uncertainties of ~4 km at 35 km depth and major normal fault has an uncertainty of ~2 km at 10 km depth that increases to 3 km at ~35 km depth (Supplementary Fig. 9).

Code availability. The tomography codes employed in this study are available online (JIVE3D⁴³, <http://bullard.esc.cam.ac.uk/~hobro/jive3D>; RAYINVR⁴⁴, <http://terra.rice.edu/departments/faculty/zelt/rayinvr.html>). Maps were generated using the Generic Mapping Tools (GMT) (<http://gmt.soest.hawaii.edu>).

Data availability. All ALEUT seismic and bathymetric data are available through the Marine Geoscience Data System (<http://www.marine-geo.org/tools/entry/MGL1110>). Data from the OBS is archived at the Incorporated Research Institutions for Seismology (IRIS) Data Management Center (DMC) (<http://ds.iris.edu/ds/nodes/dmc>) under temporary network code ZF and assembled data set ID 11-024. Temporary broadband land stations are archived under the temporary network code XM (2011).

References

- Choo, J., Downton, J. & Dewar, J. Lift: A new and practical approach to noise and multiple attenuation. *First Break* **22**, 39–44 (2004).
- Caress, D. W. & Chayes, D. N. New software for processing sidescan data from sidescan-capable multibeam sonars. In *Proc. IEEE Oceans 95 Conf.* 997–1000 (MTS/IEEE, 1995).
- Hobro, J. W. D., Singh, S. C. & Minshull, T. A. Three-dimensional tomographic inversion of combined reflection and refraction seismic traveltimes data. *Geophys. J. Int.* **152**, 79–93 (2003).
- Zelt, C. A. & Smith, R. B. Seismic traveltimes inversion for 2-D crustal velocity structure. *Geophys. J. Int.* **108**, 16–34 (1992).
- Janiszewski, H. A., Abers, G. A., Shillington, D. J. & Calkins, J. A. Crustal structure along the Aleutian island arc: new insights from receiver functions constrained by active-source data. *Geochem. Geophys. Geosyst.* **14**, 2977–2992 (2013).
- Abers, G. A. 3-dimensional inversion of regional p and s arrival times in the East Aleutians and sources of Subduction Zone Gravity Highs. *J. Geophys. Res.* **99**, 4395–4412 (1994).
- Wiemer, S. & Wyss, M. Minimum magnitude of completeness in earthquake catalogs: examples from Alaska, the western United States, and Japan. *Bull. Seismol. Soc. Am.* **90**, 859–869 (2000).